Organic enrichment in droplet residual particles relative to out of cloud over the northwest Atlantic: Analysis of airborne ACTIVATE data

Hossein Dadashazar[1], Andrea F. Corral[1], Ewan Crosbie[2,3], Sanja Dmitrovic[4], Simon Kirschler[5,6], Kayla McCauley[7], Richard Moore[2], Claire Robinson[2,3], Joseph Schlosser[1], Michael Shook[2], K. Lee Thornhill[2], Christiane Voigt[5,6], Edward Winstead[2,3], Luke Ziemba[2], Armin Sorooshian[1,4,7]

[1]Department of Chemical and Environmental Engineering, University of Arizona, Tucson, AZ, USA
[2]NASA Langley Research Center, Hampton, VA, USA
[3]Science Systems and Applications, Inc., Hampton, VA, USA
[4]James C. Wyant College of Optical Sciences, University of Arizona, Tucson, AZ, USA
[5]Institute of Atmospheric Physics, German Aerospace Center
[6]Institute of Atmospheric Physics, University Mainz, Germany
[7]Department of Hydrology and Atmospheric Sciences, University of Arizona, Tucson, AZ, USA

[*]Correspondence to: Hossein Dadashazar (hosseind@arizona.edu)

Section S1. Discussion of Figure S1

A motivation of this study is the opposite annual pattern of N_d and aerosol parameters shown in Figure S1a. Notable is that sulfate AOD exceeds that of organic AOD for all months based on MERRA-2 data, which has been shown before in the region (Braun et al., 2021). The ACTIVATE airborne data show that while the total concentrations of both aerosol components are higher in the summer months (similar to related aerosol parameters in Figure S1a), a difference compared to MERRA-2 speciated AODs is that organic levels exceed those of sulfate (except January in MBL), regardless of whether the data were in the marine boundary layer (i.e., BBL and BCB legs) or free troposphere (i.e., ACT and ABL legs) (Figure S1b). Hegg et al. (1997) concluded for the month of June based on a chemical apportionment study using aerosol column optical depth data off the mid-Atlantic coast Of the United States that the three most abundant components (in decreasing order) were water, carbonaceous compounds, and then sulfate. This is an important result with implications for aerosol characteristics such as hygroscopicity. For instance, higher organic:sulfate mass ratios in the marine boundary layer correspond to suppressed hygroscopic growth factors at high relative humidities (≥ 85%) (Hersey et al., 2009). For comparison, airborne measurements in winter and summer periods over the eastern North Atlantic showed sulfate concentrations exceeding those of organics up to the same altitudes (~1.6 km) in this study (Wang et al., 2022).

Table S1. Standard deviations and the number of points for parameters measured by the AMS instrument. Note that numbers of points refer to entire legs for which calculations were conducted using raw data rather than the raw data points per leg. Non-CAO and CAO categories include samples collected between January and March. CVI = droplet residual particle measurements in cloud; BCB = below cloud base, ACT = above cloud top, BBL = below boundary layer top, ABL = above boundary layer top. Corresponding average values are provided in Table 1 of the manuscript.

	(Non-CAO/CAO/May-Jun/Aug-Sep)				
	CVI	BCB	ACT	BBL	ABL
Organic (μg m^{-3})	-	0.63/0.43/1.84/3.93	1.06/0.14/5.08/4.50	2.13/0.69/2.58/3.25	1.01/0.57/3.92/5.86
Sulfate (μg m^{-3})	-	0.52/0.50/0.68/0.83	0.45/0.16/1.04/1.30	0.38/0.35/0.53/0.82	0.27/0.42/0.71/2.10
Nitrate (μg m^{-3})	-	0.82/0.44/0.07/0.16	0.37/0.07/0.27/0.15	1.05/0.82/0.19/0.18	0.25/0.48/0.25/0.18
Ammonium (μg m^{-3})	-	0.52/0.33/0.25/0.37	0.32/0.08/0.50/0.45	0.58/0.50/0.22/0.38	0.21/0.36/0.35/0.67
Chloride (μg m^{-3})	-	0.03/0.02/0.02/0.03	0.05/0.01/0.02/0.03	0.06/0.01/0.02/0.02	0.01/0.01/0.01/0.02
$Organic_{MF}$	0.15/0.16/0.18/0.20	0.14/0.11/0.21/0.23	0.21/0.15/0.21/0.21	0.16/0.09/0.15/0.16	0.17/0.15/0.18/0.23
$Sulfate_{MF}$	0.12/0.14/0.13/0.12	0.15/0.15/0.21/0.22	0.18/0.16/0.18/0.19	0.15/0.07/0.16/0.18	0.15/0.16/0.17/0.22
$Nitrate_{MF}$	0.05/0.06/0.06/0.05	0.10/0.08/0.01/0.02	0.09/0.07/0.03/0.03	0.08/0.11/0.02/0.02	0.04/0.09/0.03/0.02
$Ammonium_{MF}$	0.10/0.09/0.10/0.14	0.06/0.06/0.05/0.07	0.10/0.08/0.08/0.09	0.05/0.04/0.04/0.04	0.08/0.06/0.04/0.05
$Chloride_{MF}$	0.08/0.08/0.08/0.14	0.01/0.01/0.01/0.01	0.02/0.01/0.01/0.02	0.01/0.01/0.01/0.01	0.01/0.05/0.00/0.00
f_{44}	0.14/0.21/0.51/0.59	0.12/0.04/0.07/0.11	0.19/0.11/0.09/0.11	0.02/0.04/0.03/0.04	0.09/0.03/0.03/0.08
no. points	180/96/386/228	32/21/70/41	31/22/67/41	24/8/45/27	24/12/97/53

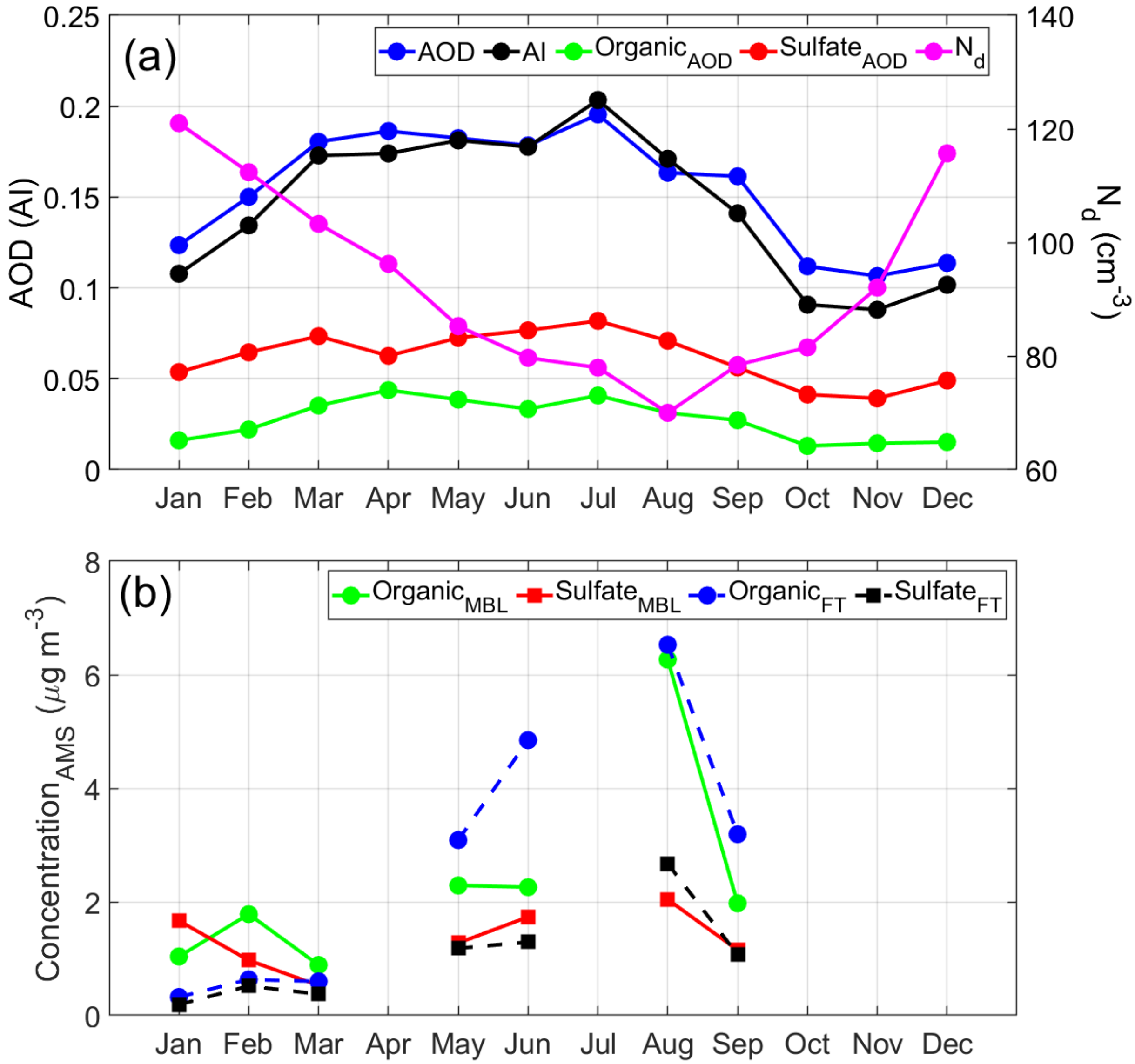

Figure S1. (a) Monthly mean values (January 2013 – December 2017) of CERES-MODIS cloud droplet number concentration (N_d) for low-level clouds (heights below 700 hPa), MERRA-2 aerosol index, and MERRA-2 total and speciated (sulfate and organic) aerosol optical depth. Data used apply to the spatial area over the northwest Atlantic where ACTIVATE data were collected (boxes 1-3 in Figure 1). (b) Monthly mean values of sulfate and organic using ACTIVATE airborne data differentiated by marine boundary layer (BCB/BBL legs) versus free troposphere (ACT/ABL legs).

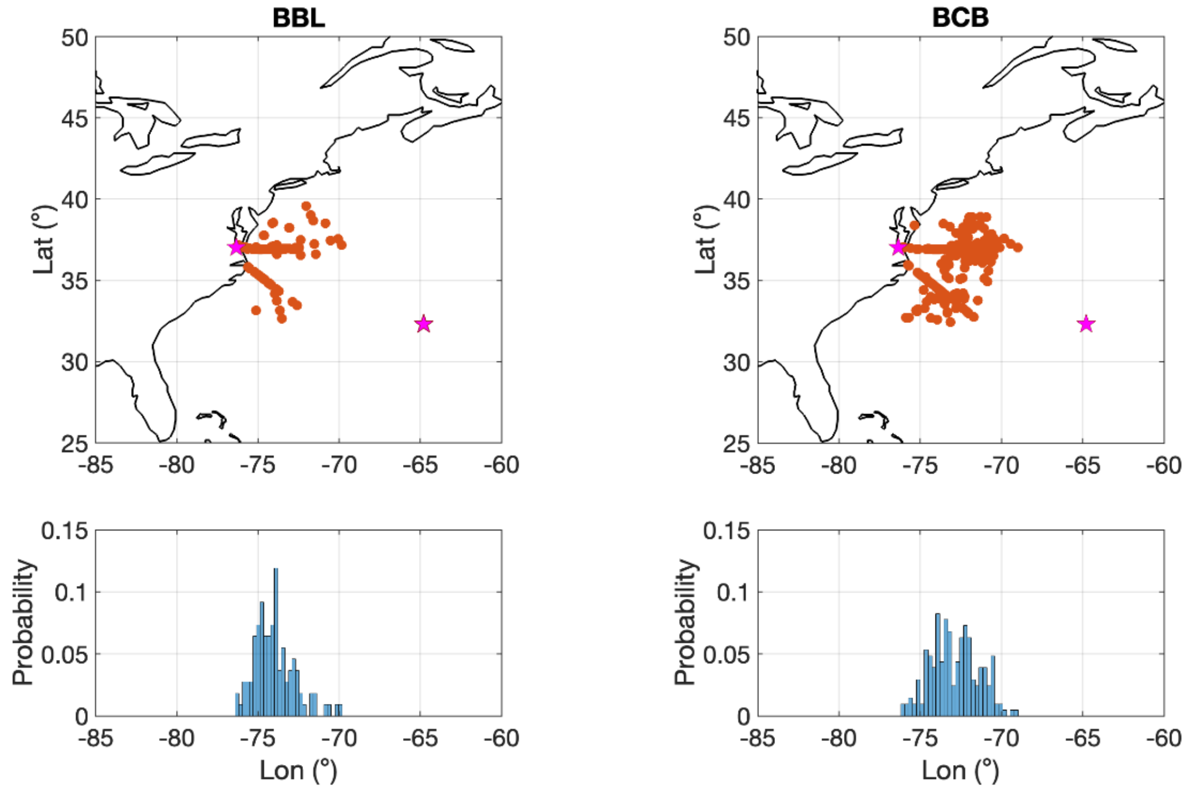

Figure S2. Midpoint locations of both below bounday layer top (BBL) legs in cloud-free ensembles and below cloud base (BCB) legs in cloudy ensembles during ACTIVATE's deployments 1-4 in 2020 and 2021. The bottom panels show probability histograms of the location of the two leg types relative to longitude. The analagous results for above boundary layer top (ABL) and above cloud top (ACT) legs resemble these since the ABL and ACT legs occur fairly soon after BBL and BCB legs, respectively, within an ensemble. The pink stars represent NASA Langley Research Center (Hampton, Virginia) and Bermuda for reference.

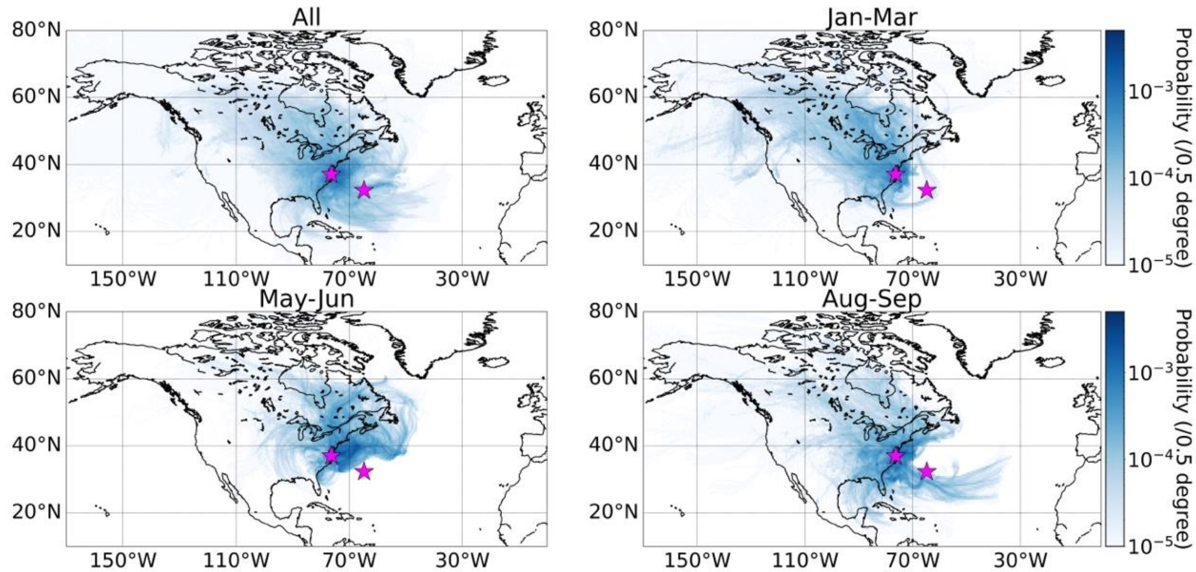

Figure S3. Five day back-trajectory probability distribution maps ending at the point of the Falcon aircraft during ACTIVATE flights for the time stamps coinciding with 29,164 cloud-free AMS data points. "All" shows the cumulative results of the other three panels. The January-March panel combines CAO and non-CAO days, which are separated for other parts of the study. The pink stars represent NASA Langley Research Center (Hampton, Virginia) and Bermuda for reference.

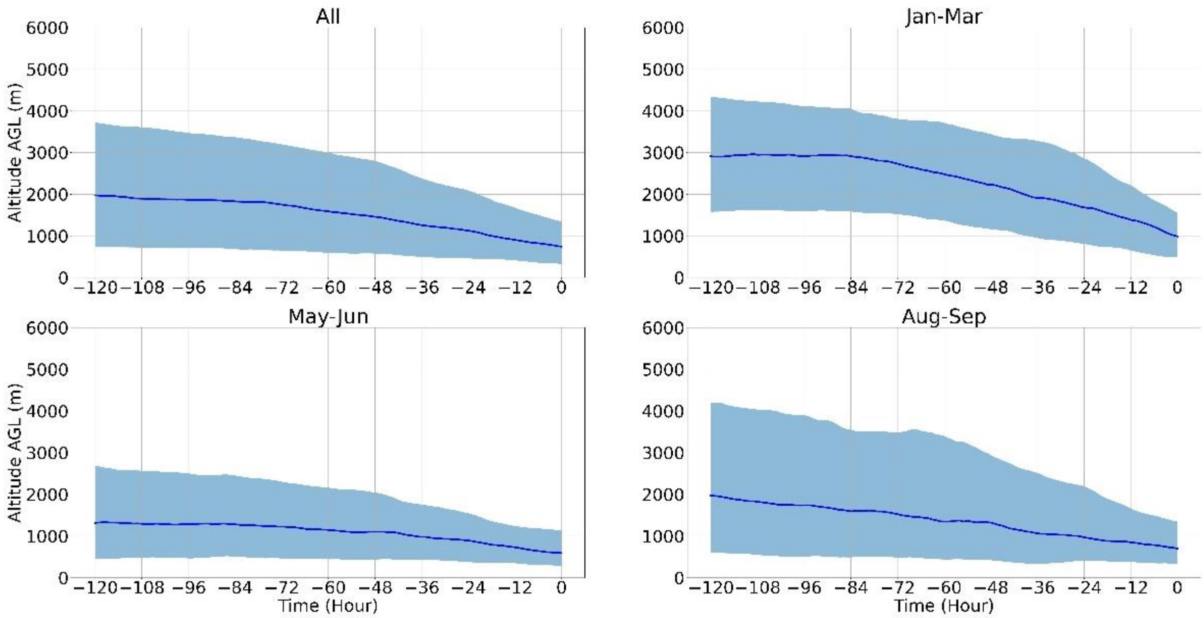

Figure S4. Altitude history of trajctories corresponding to Figure S3. The solid line represents the median and the shading corresponds to the $25^{th}/75^{th}$ percentiles. "All" shows the cumulative results of the other three panels. The January-March panel combines CAO and non-CAO days, which are separated for other parts of the study.

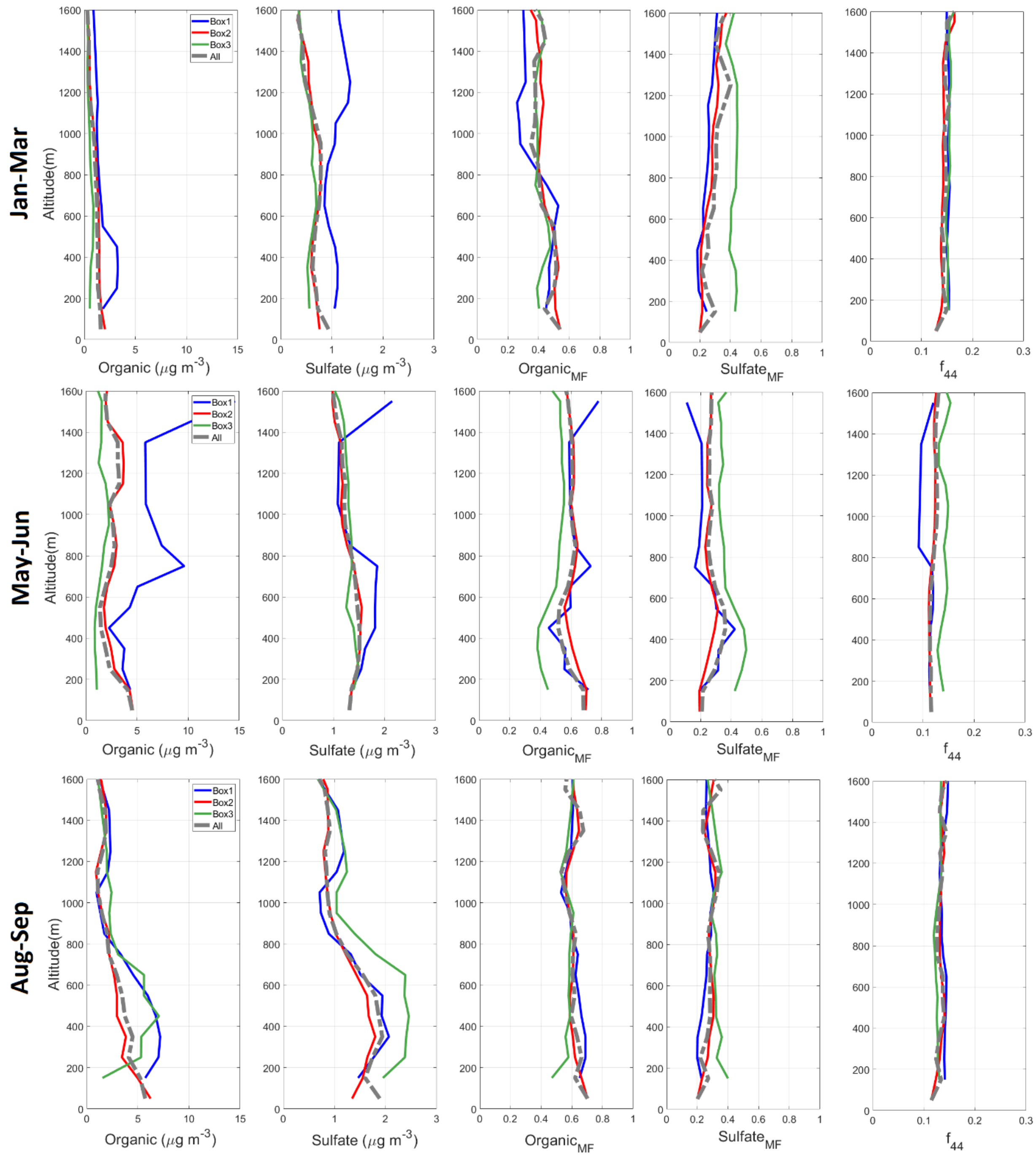

Figure S5. Vertically-resolved cloud-free AMS data for the different time periods of ACTIVATE deployments and boxes defined in Figure 1. Shown are (left to right) organic and sulfate concentrations, organic and sulfate mass fraction, and the ratio of m/z 44 to total organic (f_{44}). The top row for January-March combines CAO and non-CAO days, which are separated for other parts of the study.

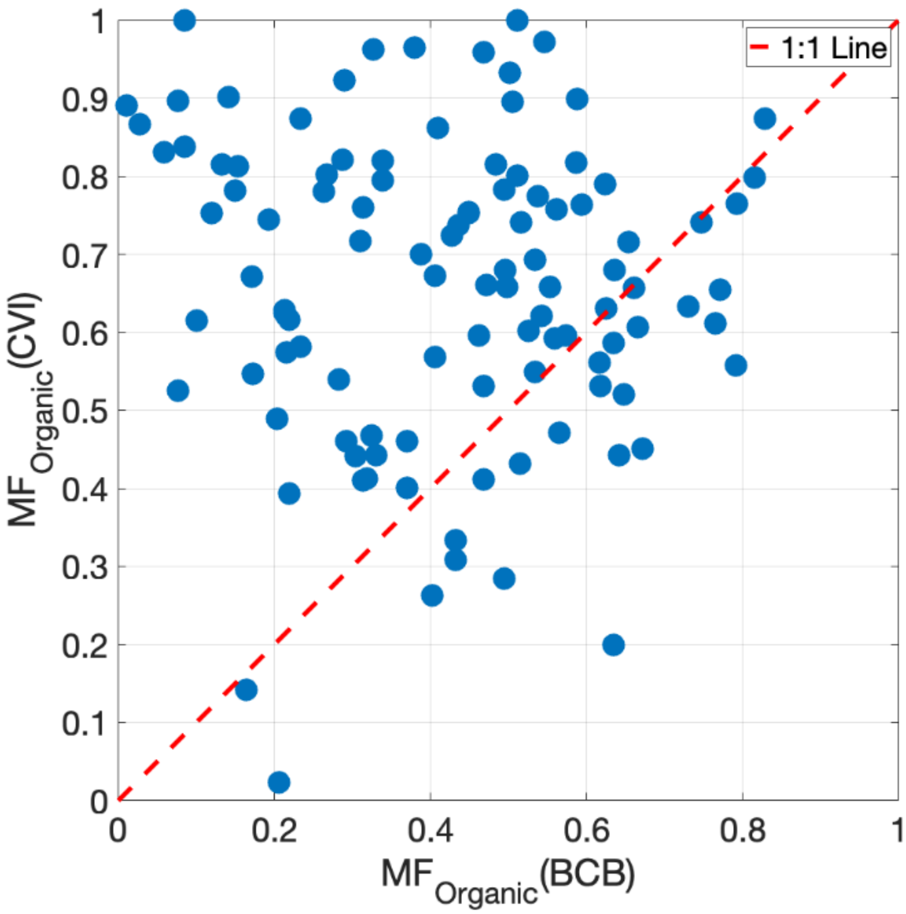

Figure S6. Scatterplot of organic mass fraction in droplet residuals (downstream CVI in cloud) and in aerosol sampled during the closest below cloud base (BCB) leg from ACTIVATE deployments 1-4. A total of 25 points out of a total of 110 (23%) were below the 1:1 line.

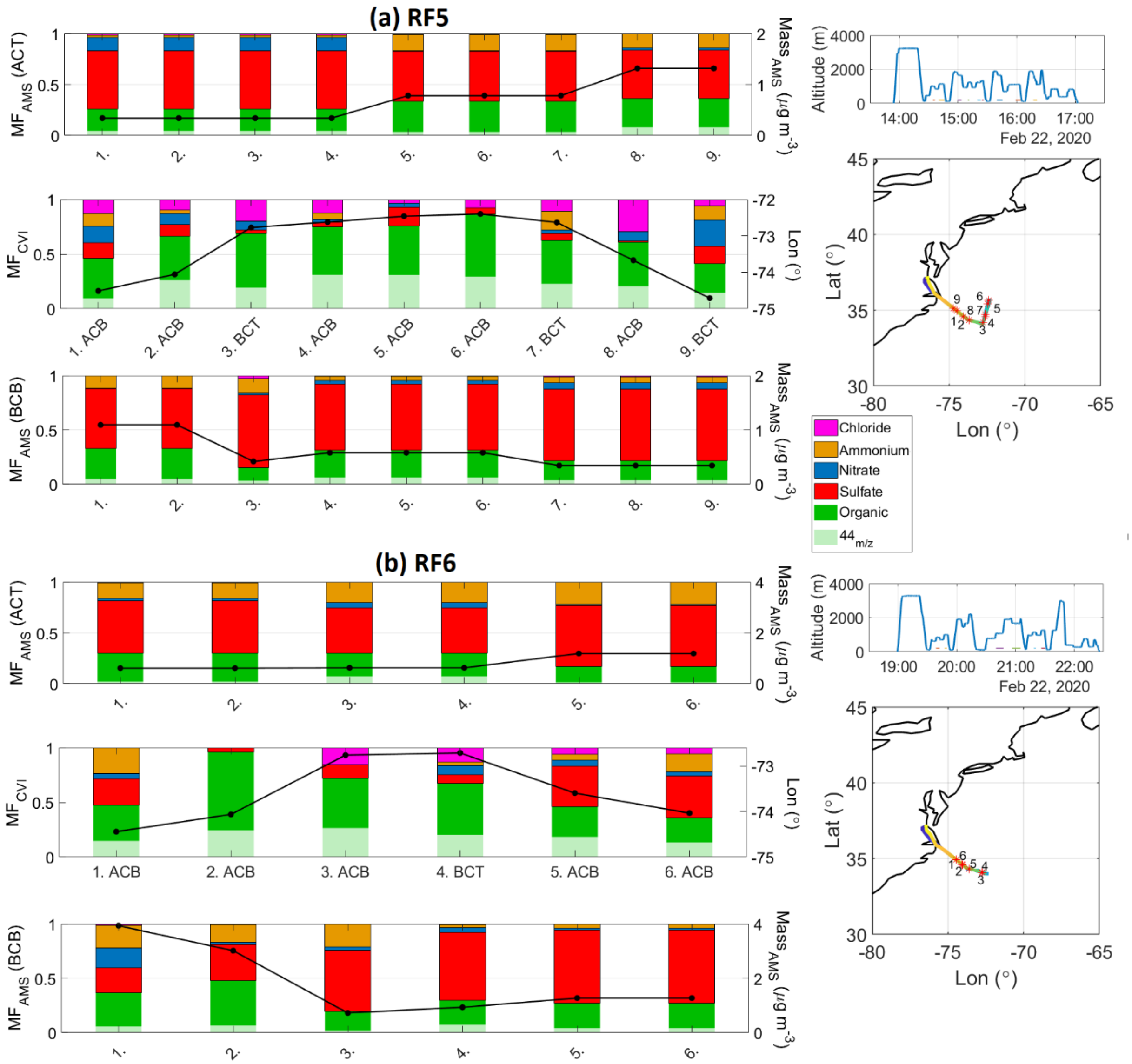

Figure S7. Summary of AMS composition in adjacent BCB, cloud, and ACT legs during back-to-back flights (Research Flights 5 and 6) in cold air outbreak conditions on 22 February 2020. Shown in the bar charts are the mass fractions of AMS components in addition to either total AMS mass (for ACT and BCB legs; such data are not robust for CVI legs due to how the CVI operates) or longitude on the right y-axis. Note that some BCB and ACT legs are repeated for different cloud legs as they represent the closest leg to an individual cloud leg. On the far right are flight altitude time series along with the spatial map with numbers corresponding to the leg numbers in the bar charts.

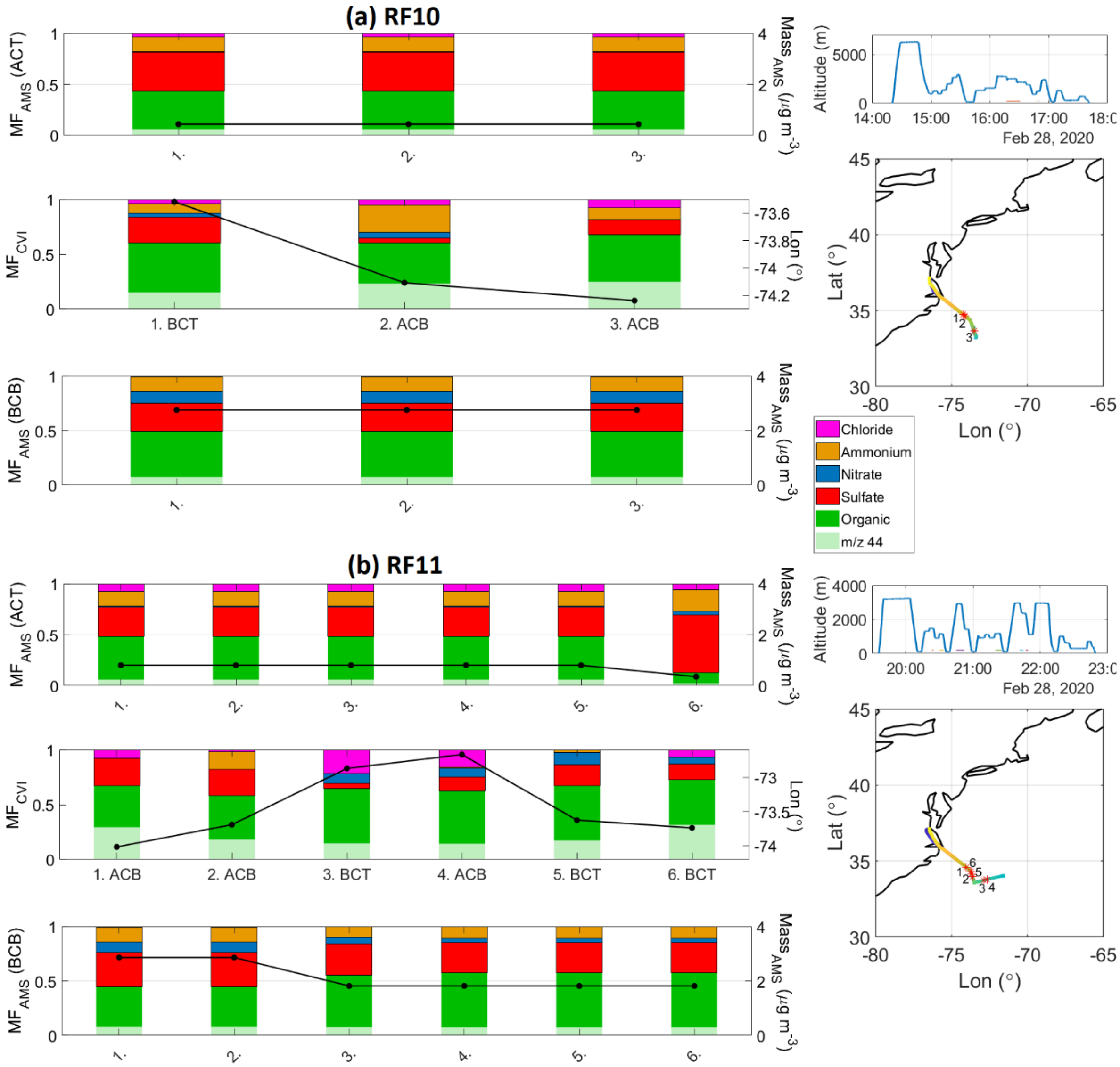

Figure S8. Summary of AMS composition in adjacent BCB, cloud, and ACT legs during back-to-back flights (Research Flights 10 and 11) in cold air outbreak conditions on 28 February 2020. Shown in the bar charts are the mass fractions of AMS components in addition to either total AMS mass (for ACT and BCB legs; such data are not robust for CVI legs due to how the CVI operates) or longitude on the right y-axis. Note that some BCB and ACT legs are repeated for different cloud legs as they represent the closest leg to an individual cloud leg. On the far right are flight altitude time series along with the spatial map with numbers corresponding to the leg numbers in the bar charts.

References

Braun, R. A., McComiskey, A., Tselioudis, G., Tropf, D., and Sorooshian, A.: Cloud, Aerosol, and Radiative Properties Over the Western North Atlantic Ocean, Journal of Geophysical Research: Atmospheres, 126, e2020JD034113, https://doi.org/10.1029/2020JD034113, 2021.

Hegg, D. A., Livingston, J., Hobbs, P. V., Novakov, T., and Russell, P.: Chemical apportionment of aerosol column optical depth off the mid-Atlantic coast of the United States, J Geophys Res-Atmos, 102, 25293-25303, 1997.

Hersey, S. P., Sorooshian, A., Murphy, S. M., Flagan, R. C., and Seinfeld, J. H.: Aerosol hygroscopicity in the marine atmosphere: a closure study using high-time-resolution, multiple-RH DASH-SP and size-resolved C-ToF-AMS data, Atmos. Chem. Phys., 9, 2543-2554, 10.5194/acp-9-2543-2009, 2009.

Wang, J., Wood, R., Jensen, M. P., Chiu, J. C., Liu, Y., Lamer, K., Desai, N., Giangrande, S. E., Knopf, D. A., Kollias, P., Laskin, A., Liu, X., Lu, C., Mechem, D., Mei, F., Starzec, M., Tomlinson, J., Wang, Y., Yum, S. S., Zheng, G., Aiken, A. C., Azevedo, E. B., Blanchard, Y., China, S., Dong, X., Gallo, F., Gao, S., Ghate, V. P., Glienke, S., Goldberger, L., Hardin, J. C., Kuang, C., Luke, E. P., Matthews, A. A., Miller, M. A., Moffet, R., Pekour, M., Schmid, B., Sedlacek, A. J., Shaw, R. A., Shilling, J. E., Sullivan, A., Suski, K., Veghte, D. P., Weber, R., Wyant, M., Yeom, J., Zawadowicz, M., and Zhang, Z.: Aerosol and Cloud Experiments in the Eastern North Atlantic (ACE-ENA), Bulletin of the American Meteorological Society, 103, E619-E641, 10.1175/bams-d-19-0220.1, 2022.